IMECE2008-66225

ATOMIZATION CHARACTERISTICS, GLOBAL EMISSIONS, AND TEMPERATURE IN BIOFUEL AND PETROLEUM FUEL SPRAY FLAMES

Jaime A. Erazo Jr.
University of Oklahoma
Norman, OK, USA

R.N. Parthasarathy
University of Oklahoma
Norman, OK, USA

S.R. Gollahalli
University of Oklahoma
Norman, OK, USA

ABSTRACT

Spray flame characteristics of canola methyl ester biofuel (CME) and petroleum fuel (No. 2D) are described. An enclosed spray flame in a heated co-flow air environment at ambient pressure was studied. A single nozzle, swirl-type, air-blast atomizer with a nozzle diameter of 300 microns was used to create the spray. The spray droplet size and velocity distributions were measured using a two-component phase Doppler particle analyzer. In-flame temperature profiles were measured using a type-R thermocouple. Global emission indices of NO and CO were derived from concentration measurements in the combustion products. The overall equivalence ratio was kept at 0.75 to simulate lean burning conditions. The changes in atomization air flow rate produced similar changes in atomization characteristics of both fuels. Emission indices of NO and CO for petroleum fuel were higher than those of the CME fuel. In-flame temperature levels were lower for the CME fuel than for the petroleum fuel at corresponding flame locations.

NOMENCLATURE

CME- Canola methyl ester
D_{32}- Sauter mean diameter
NDIR—Nondispersive infrared
PDPA- Phase Doppler particle analyzer
T_{cf}= Air co-flow temperature
V_f= Volumetric flow rate of fuel
V_{aa}= Volumetric flow rate of atomization air
V_{cf}= Volumetric flow rate of air co-flow

INTRODUCTION

Biofuels have recently emerged as potentially viable alternatives to petroleum fuels. They have has essentially zero sulfur content, are renewable, and are considered carbon-neutral from the environmental considerations [1]. However, some diesel engine studies [2,3,4] have reported as much as 14% increase in NO_x emissions when burning biofuel in place of petroleum fuel. It was found that an increase in Iodine number caused higher NO_x emissions in biofuel engines [2].. One recent suggestion is that the presence of double bonds in the biofuel increases flame temperature and subsequently NO_x emissions [5]. Among other reasons cited for increased NO_x emissions is the bulk modulus difference between biofuel and No. 2D, which have been shown to affect injection timing [6].

Based on several laser imaging studies Dec [7] has shown that the mechanism and process of combustion in diesel engines are drastically different from those in continuous combustion devices, and the earlier spray combustion models presented by Faeth [8] are not applicable to diesel engines. Hence, the NO emission increase found with biofuels in diesel engines may not occur in continuous combustion devices.

The purpose of our research program was to investigate the application of biofuels in continuous combustion devices such as residential and utility furnaces, or gas turbines. The complexity of the full-scale combustors makes it very difficult to study individual aspects of the combustion process that result

in changes of NO_x emissions. The effects of parameters such as swirl and combustor geometry are interconnected and cannot be easily isolated. Hence, simpler burner studies in controlled environments have been undertaken. Laminar flame studies have been conducted to isolate the effects of fuel chemistry in the present authors' laboratory [8]. A controlled spray flame study is useful to extend the laminar flame results closer to that of practical combustors, and to provide more insight into the combustion characteristics of biofuels, which is the subject of this paper.

The specific objective of this paper was to investigate the differences between petroleum and biofuels on the atomization characteristics and combustion emissions in a spray flame environment. No. 2 petroleum fuel and neat canola methyl ester biofuel were used. Global equivalence ratio, droplet size, and air temperature were controlled. Spray flame characteristics, droplet size, mean axial/radial velocity of droplets, global emissions of carbon monoxide and nitric oxides, and in-flame temperature were measured.

EXPERIMENTAL APPARATUS

The experiments were carried out in a large steel combustion chamber (76 cm by 76 cm and 143 cm in height), as shown in Figure 1. Combustion air was drawn from the lab air-supply facilities and was dehydrated/filtered before passing through a 10 kW air heater. Insulated steel piping guided the air into a stainless steel flow settling chamber, which was filled with marbles to provide a uniform flow of air into the test section (Fig. 2). The test section was a stainless steel unit with four Vycor glass windows to provide optical access to the spray flame.

The fuel tank and atomizing air system were connected to the test section through a settling chamber. An air-blast atomizer nozzle was used as the injector. The nozzle was positioned in the test section at the tip of a stainless steel tube. Atomization air stream was passed through a concentric pipe. Fuel tank was pressurized with nitrogen. Figures 3 and 4 show the fuel and atomization-air supply systems and the photograph of the fuel-nozzle. Air heater used a controller to maintain a steady co-flow temperature.

A 2-channel phase Doppler particle analyzer was used to measure axial and radial components of velocity and diameter of droplets in the spray flame. The beam from an argon-ion laser was passed through a color separator to obtain two beams of wavelength 514 nm and 488 nm (green and blue), and each was split into two beams. The beams were passed through fiber optic cables to the transmitting optics. A forward scattering scheme (30^0 off axis) was used to collect the scattered light from the probe volume. The focal length of the transmitting and receiving optics was 500 mm.

Fringe spacing in the probe volume was approximately 12.86 μm for both sets of beams. Prior to this study, the system was calibrated using a monodisperse droplet generator. Measurement of reverse flow was possible through the use of frequency shifting of one beam of each color. In general, 10,000 data points were collected at each measurement location. Usually data collection was completed within 120 seconds for a given measurement. Some regions of the spray flame required more time for collection

The PDPA transmitter and receiver were mounted on 3-way traverses, which provided motion in three directions. Since the spray flame appeared symmetric about the centerline radial profiles for only one half of the spray flame are presented. The measurement locations within the spray flame are given in Figure 5.

The species concentrations were measured with a four gas analyzer (CO_2 and CO with NDIR detectors, NO and O_2-with electrochemical sensors). An uncooled quartz probe with 1 mm tip diameter was used to collect the gas samples. A quartz funnel with an open bottom positioned at the exit of the test section was used to mix and direct the flow into the probe. A moisture condenser and a fiber glass air filter were used to treat the samples before they were admitted into the analyzers. The following equation was used to calculate emission index [8], where x_i is the mole fraction of the species i, x is the number of carbon atoms in a molecule of fuel, x_{CO} and x_{CO2} are the mol fractions of CO and CO_2, and MW is the molecular weight.

$$ EI_i = \left(\frac{X_i}{X_{CO} + X_{CO_2}} \right) \cdot \left(\frac{x \cdot MW_i}{MW_F} \right) $$

Flame temperature was measured with a type R (Pt/Pt-Rh-13%) unshielded thermocouple (0.35 mm bead diameter). The thermocouple was mounted on a traverse which provided horizontal and vertical motion. Thermocouple readings were corrected for radiation and conduction errors [9]. Flame temperature was measured at axial locations 25%, 50% and 75% of the visible flame length away from the burner. Access to the flame was facilitated by the use of two custom cut Vycor glass pieces which provided a narrow slit just wide enough for the insertion of the thermocouple. Data acquisition was accomplished using LabView software installed in a personal computer.

A global equivalence ratio of approximately 0.75 was used to simulate a lean-burning combustor. Properties of the two fuels are provided in Table 1. Canola methyl ester fuel has a higher final boiling point and a narrower distillation temperature range than the petroleum fuel. Table 2 provides the fuel and atomization–air flow rates and temperature settings.

PDPA measurements were repeated on different days. Temperature measurements were averaged over 100 samples each day. Emission measurements were repeated 3-4 times each day. The uncertainty levels were calculated using t-test at 95% confidence level. The uncertainty bars of propagated errors are shown in figures.

RESULTS AND DISCUSSION

Atomization Characteristics

The effects of atomization air-flow rate on the radial profiles of the droplet Sauter Mean Diameter (SMD) at different axial locations in the spray flames of No. 2 petroleum fuel are presented in Fig 6. The corresponding data in CME sprays are presented in Fig.7. The Sauter mean diameter increases with radial distance due to the centrifugal effect of the swirl. A 20% increase in atomization air-flow rate in petroleum fuel spray causes approximately 10% decrease in the peak diameter of droplets at the exit of the atomizer and downstream However, in CME spray the effect of atomization air flow rate although seems larger at the nozzle exit, similar effect is noticed away from the nozzle. Also, in CME spray the changes in the SMD with the distance from the nozzle appear small. This is attributed to narrower distribution of droplet SMD in CME biased towards large droplets due to higher viscosity of biofuel. Further, the SMD at the downstream locations of CME spray is smaller indicating a higher evaporation rate. This is in conformity with the evaporation constant measurements of n-petroleum and biofuels stated in [10].

The radial profiles of the axial and radial components of the mean velocity of droplets are plotted in Figures. 8-9 for petroleum fuel and in Figures 10-11 for biofuel. In both sprays, the axial component of droplet velocity in the petroleum fuel spray peaks at the centerline and gradually decreases in the radial direction. The spray width increases while the peak axial velocity decreases away from the burner. The radial component of velocity increases in the radial direction due to the swirling atomizing air inside the nozzle. The spray flame width, determined by the boundary where the droplets are absent, reduces with a decrease in atomization air flow rate. At high atomization flow rate, droplets are detected until 1.75 cm in the radial direction whereas at the small flow rate condition data collection had to be stopped at 1.5 cm due to a lack of drops detected by the PDPA.

Larger atomization flow rate results in a larger component of axial velocity at the exit of the atomizer and the effect seems to carry over for the downstream locations. This result occurs for both fuels.

The CME spray flame produces similar shapes of mean droplet axial and radial velocity profiles. Although there is no significant difference in the axial component of velocity at the exit of the injector, presumably due to the same atomizing air flow rate, at downstream locations CME droplets move faster due to smaller SMD that enables them to follow flame gases without significant slip. The radial velocity components confirm these results with smaller values in CME spray.

Flame Temperature Profiles

Figures 12 and 13 show the radial profiles of flame temperature in No.2D and CME spray flames at two atomization air-flow rates. In the near burner region (25% of flame length away from the nozzle), the increase of atomizing air does not produce a significant effect on the peak temperature in No. 2D spray flame, whereas in the far-burner region (75% flame length away from the nozzle), peak temperature is increased by 100 K at higher atomizing air flow arte. This can be attributed to higher oxygen availability in the flame core.

At the same atomization air flow rate, although the peak temperature in the near-burner region of CME flame is same as that in NO.2D flame, it drops by 200K in the far burner region. This clearly demonstrates the higher influence of homogeneous gas phase reactions due to the oxygen in biofuel molecule compared to more soot formation and accompanying heterogeneous combustion in No. 2D flame. This is further evidenced by the off-axis valley in CME flame that shows the effect of small amount of oxygen which increases endothermic pyrolysis reactions. Also, CME contains more double bonds and higher Iodine number which increases endothermicity.

Emission Indices:

Figures 14 and 15 show the effects of atomization air on the emission index of CO and NO in No. 2d and CME spray flames.

Higher atomizing air flow rate although does not affect significantly the CO emission index in No. 2D spray flame, decreases NO emission index. Smaller drops and shorter residence times at higher atomization air flow rate are the reasons for lower NO. However, the small change in atomization air flow rate does not affect the overall oxidation rate and consequently CO emission index as the soot combustion is dominant in No.2D spray flames. In CME flame, however, the emission index of both NO and CO decreases when the atomization air flow rate increases. The additional atomization air adds to the effect of the oxygen present in the fuel itself, and hence lowers the soot formation and diffusion-controlled reaction zones. The net effect is to lower both CO and NO emissions.

The emission index of CO in CME flame is higher and of NO is lower than in No. 2D flames. This observation is contrary to that observed in diesel engines [2,3,4]. However, NO emission results agree with the results of [10,11,12] in continuous combustion sprays similar to that in the present study. The lower emission of NO in CME flame in our study may be explained by the differences in the transient combustion processes in diesel engines and steady sprays simulating continuous combustors [7].

The higher CO emission in the CME flame is in contrast to that observed by [10]. The small amount of oxygen in the molecule of biofuel facilitates conversion of carbon in the fuel to CO than leaving it as soot resulting in more CO emission. However, the swirling co-flow and much higher atomizing air

3   Copyright © 2008 by ASME

flow rate (15-25% of the total air) explain the lower CO observed in [10].

SUMMARY AND CONCLUSIONS

Droplet size and velocity profiles were obtained for spray flames of No. 2D fuel and canola methyl ester (CME) biofuel. Effects of atomization air flow rate on SMD were discussed. An increase in atomization air flow rate decreased the peak SMD at the exit of nozzle and downstream. CME spray at downstream location exhibited smaller SMD indicating a higher evaporation rate. Larger atomization air flow rates produced a larger component of axial velocity. CME fuel spray flames produced similar shapes of axial and radial mean velocity profiles as those in No. 2D spray. Flame temperature profiles for the two fuels revealed that the peak temperature was 200K lower in the far-burner region of the CME spray. Diffusion controlled heterogeneous reactions dominate in the No. 2D fuel spray flame while homogenous gas phase reactions dominate in the CME spray flame. The CME spray flame produced a smaller NO emission index than No. 2D fuel spray flame. This is contrary to the observation in transient combustion in diesel engines, but agrees with steady biofuel spray flames cited earlier.

REFERENCES

1- Agarwal, A.K., "Biofuels (Alcohols and Biodiesel) Applications for Fuels in Internal Combustion Engines," **Progress in Energy and Combustion Science**, Vol. 33, 2007, pp. 233-271.

2- McCormick, R.L., Graboski, M.S., Alleman, T.L., and Herring, A.M., "Impact of Source Material and Chemical Structure on Emissions of Criteria Pollutants from a Heavy-Duty Engine," **Environmental Science and Technology**, Vol. 35, 2001, pp. 1742-1747.

3- Lin, Y., Wu, Y.G., and Chang, C.T., "Combustion Characteristics of Waste-Oil Produced Biodiesel/Diesel Fuel Blends," **Fuel**, Vol. 86, 2007, pp. 1772-1780.

4- Tat, M.E., and Van Gerpen, J.H., "Fuel Property Effects on Biodiesel," **2003 ASAE Annual International Meeting**, Paper No. 036034.

5- Ban-Weiss, G., Chen, J.Y., Buchholz, B.A., and Dibble, R.W., "A Numerical Investigation into the Anomalous Slight NO_x Increase When Burning Biodiesel; A New (Old) Theory,"
American Chemical Society, **Fuel Chemistry Division**, Vol. 51 (1), 2006, pp. 24-30.

6- Szybist, J.P., Boehman, A.L., Taylor, J.D., and McCormick, R.L., "Evaluation of Formulation Strategies to Eliminate the Biodiesel NO_x Effect," **Fuel Processing Technology**, Vol. 86, 2005, pp. 1109-1126.

7- Love, N., Parthasarathy, R.N., and Gollahalli, S.R., "A Method for the Rapid Characterization of Combustion Properties of Liquid Fuels Using a Tubular Burner," IMECE2007-42112, **International Mechanical Engineering Congress and Exposition**, Seattle, Washington, November 11-15, 2007.

8- Turns, S.R., *An Introduction to Combustion: Concepts and Applications.* McGraw-Hill Higher Education, 2nd Edition, 2000.

9- Morin, C., Chauveau, C., Dagaut, P., Gokalp, I., and Cathonnet, M., "Vaporization and Oxidation of Liquid Fuel Droplets at High Temperature and High Pressure: Application to N-Alkanes and Vegetable Oil Methyl Esters," **Combustion Science and Technology,** Vol. 176, 2004, pp. 499-529.

10- Sequera, D., and Agrawal, A.K., "Combustion Performance of Liquid Biofuels in a Swirl-Stabilized Burner," **Journal of Engineering for Gas Turbines and Power**, Vol. 130, 2008.

11- Li, L. "Experimental Study of Biodiesel Spray and Combustion Characteristics," **SAE Power train & Fluid Systems Conference and Exhibition**, Paper 2006-01-3250, October 2006.

12- Hashimoto, N., Ozawa, Y., Mori, N., Yuri, I., and Hamamatsu, T., "Fundamental Combustion Characteristics of Palm Methyl Ester as Alternative Fuel for Gas Turbines," **Fuel**, Vol. 87, 2008, pp. 3373-3378.
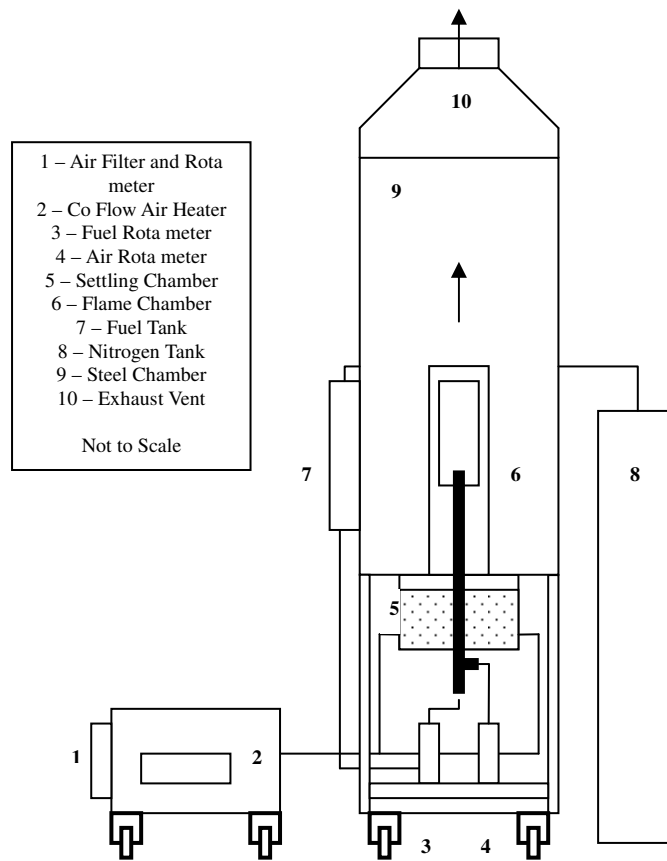
FIGURES AND TABLES

1 – Air Filter and Rota
meter
2 – Co Flow Air Heater
3 – Fuel Rota meter
4 – Air Rota meter
5 – Settling Chamber
6 – Flame Chamber
7 – Fuel Tank
8 – Nitrogen Tank
9 – Steel Chamber
10 – Exhaust Vent

Not to Scale

Figure 1- Combustion chamber schematic drawing.

Figure 2- Test Section with Vycor glass.

5   Copyright © 2008 by ASME

51.8 cm

20.3 cm

1 – Fuel Inlet
2 – Air Inlet
3 – Settling Chamber
with Marbles
4 – Screen
5 – Air Co- Flow Inlet
6 – Flame Chamber
7 – Injector
8 – Set Screw

Not to Scale
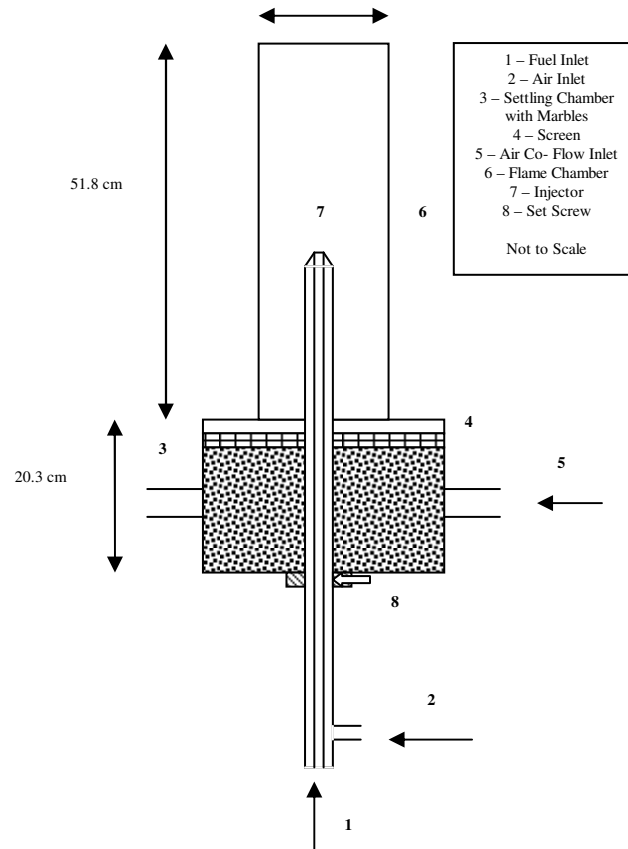
Figure 3- Schematic drawing of fuel and atomization-air systems
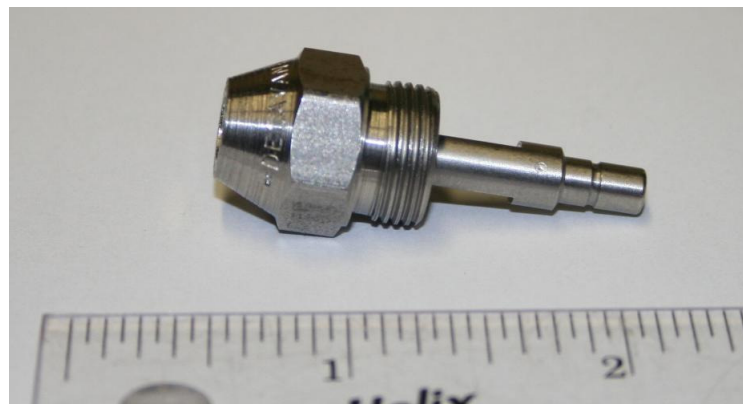
Figure 4- Air blast atomizer.
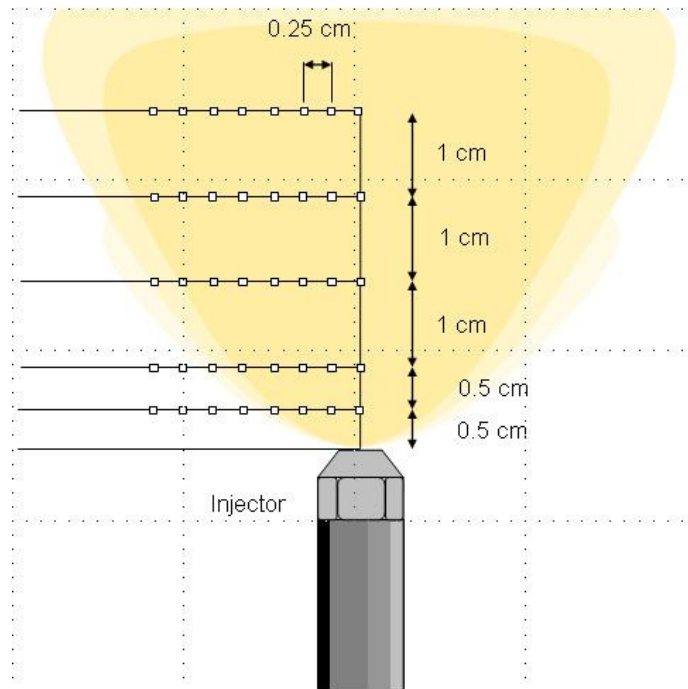
Figure 5- Description of measurement locations in the spray flame.
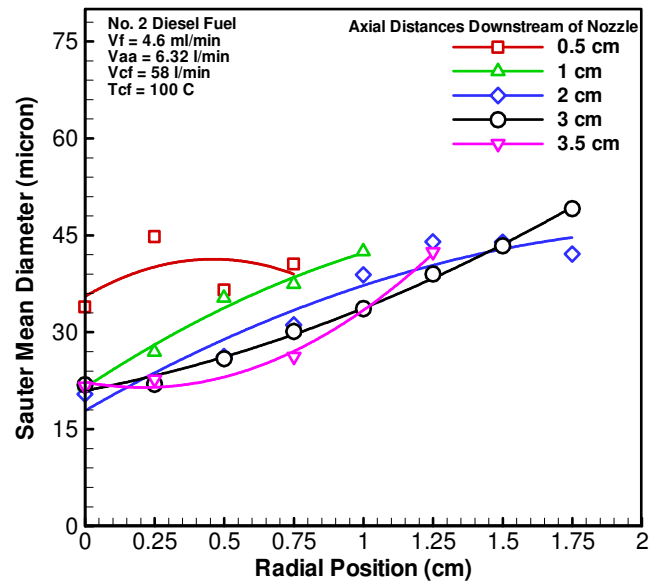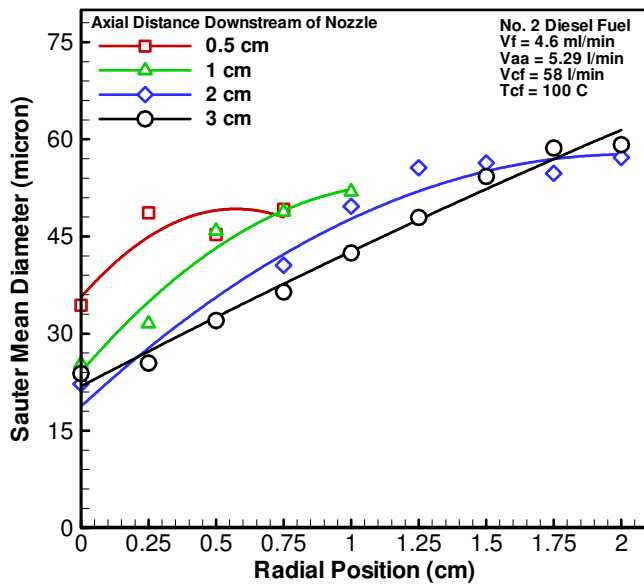
Figure 6- Effect of atomization air flow rate on SMD profiles in No. 2 D fuel spray flames. Uncertainty in these figures is approximately ± 4 microns.
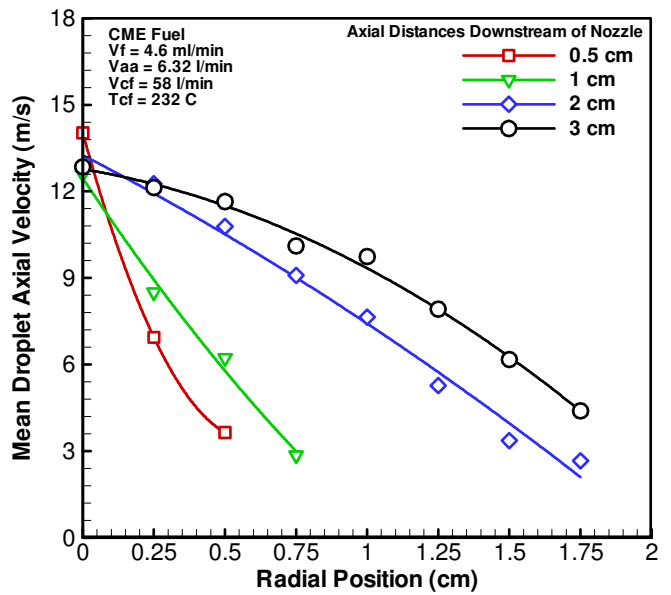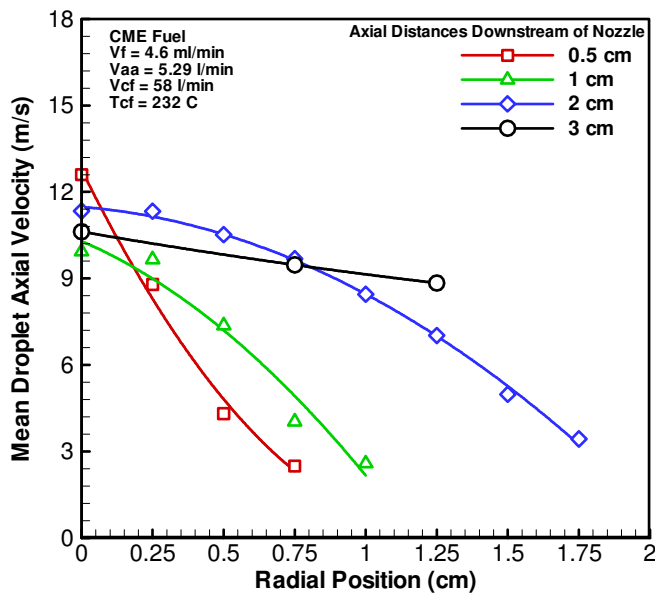
Copyright © 2008 by ASME
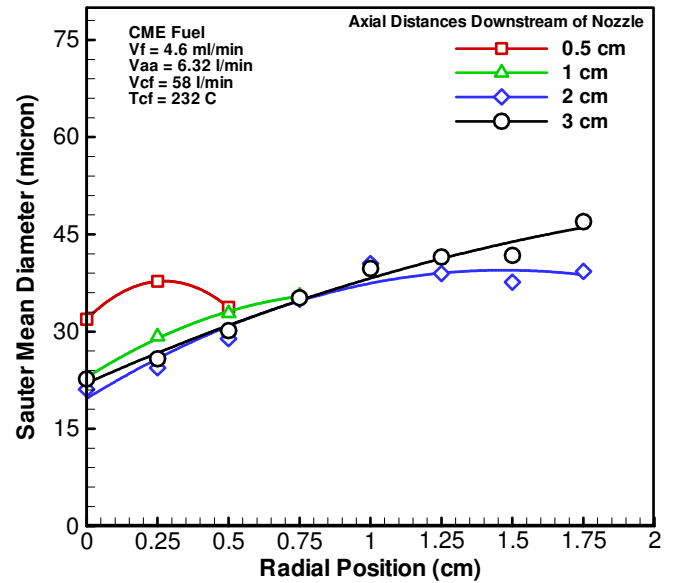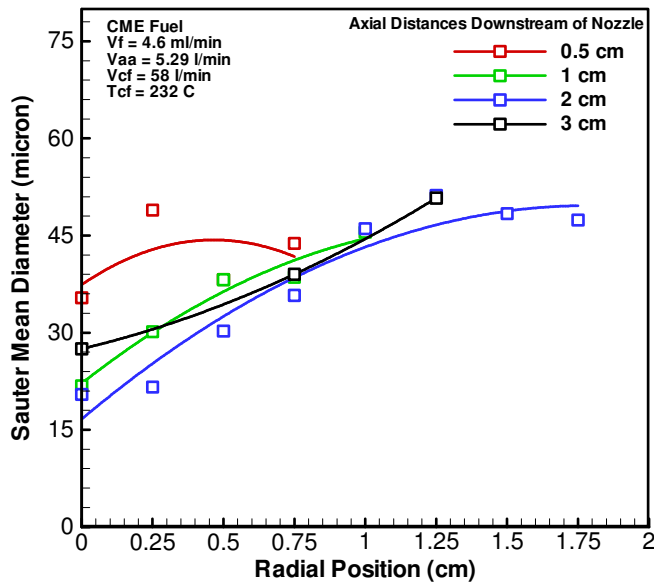
Figure 7- Effect of atomization air flow rate on SMD profiles in CME fuel spray flames. Uncertainty in these figures is approximately ± 4 microns.
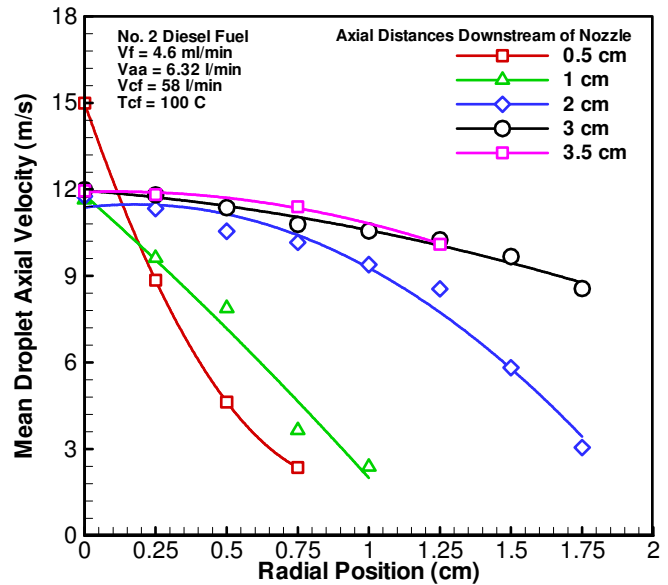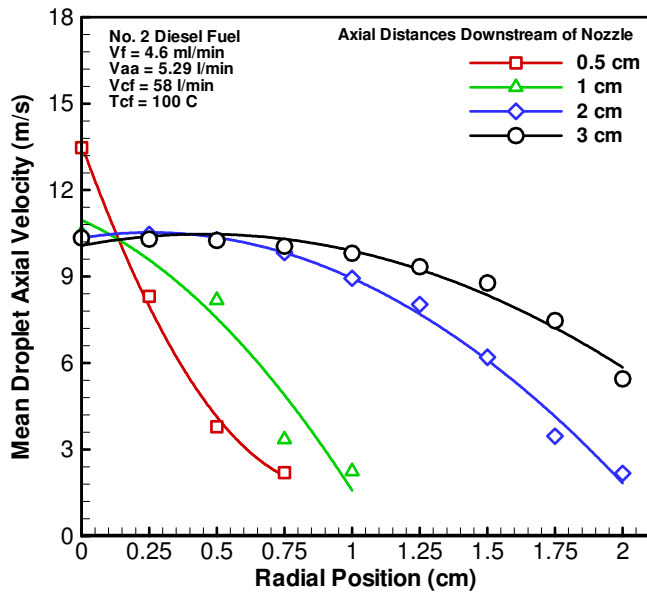
Figure 8- Effect of atomization air flow rate on mean axial velocity profiles in No. 2 D fuel spray flames. Uncertainty in these figures is approximately ± 0.21 m/s.

8

Copyright © 2008 by ASME
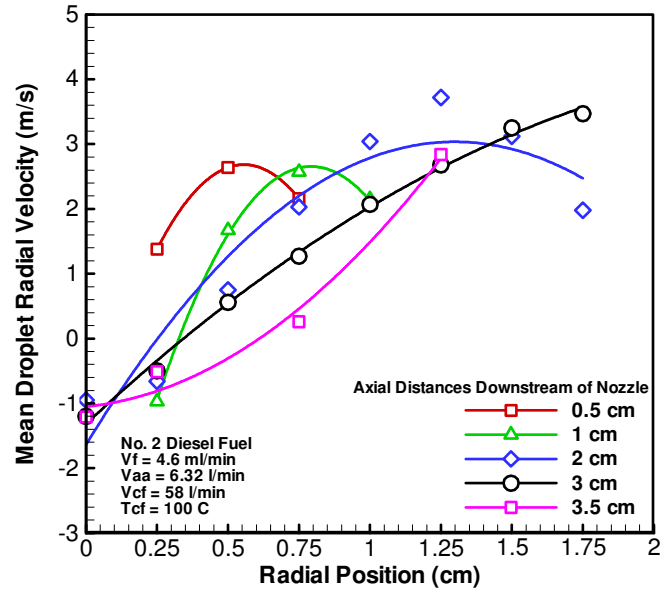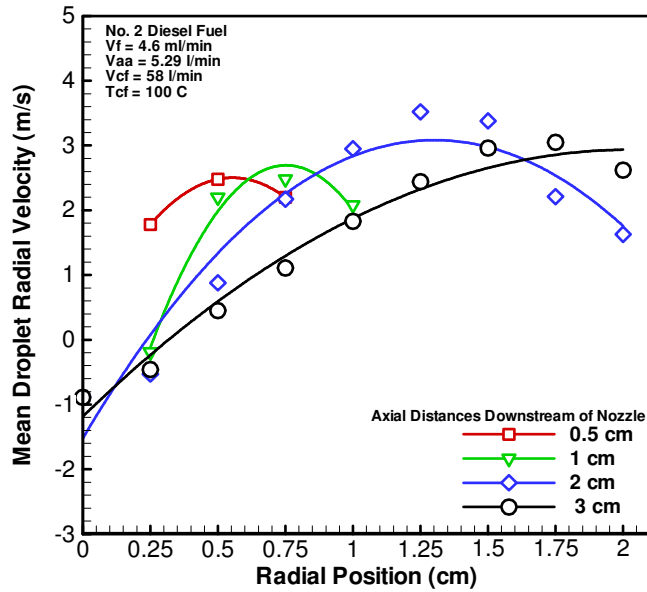
Figure 9- Effect of atomization air flow rate on mean radial velocity profiles in No. 2 D fuel spray flames. Uncertainty in these figures is approximately $\pm$ 0.17 m/s.
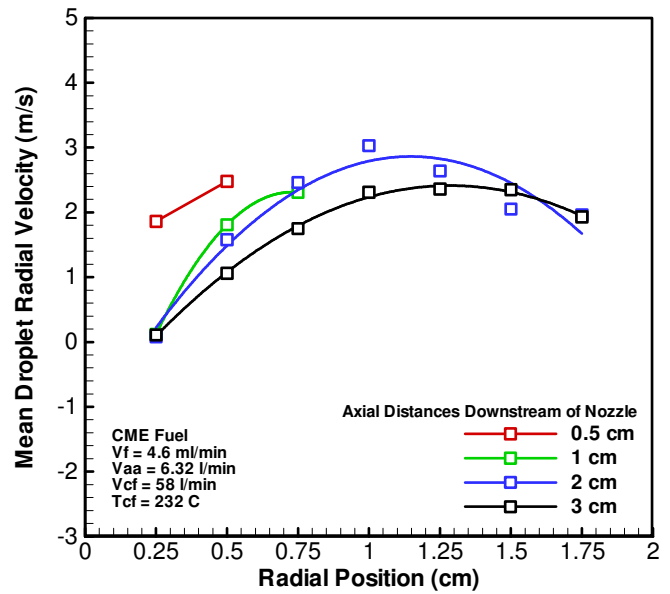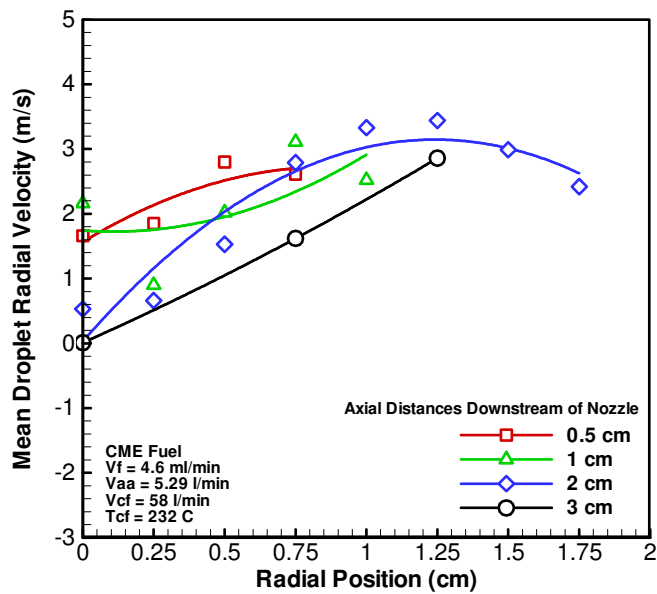

Figure 10- Effect of atomization air flow rate on mean axial velocity profiles in CME fuel spray flames. Uncertainty in these figures is approximately $\pm$ 0.2 m/s.

9

Copyright © 2008 by ASME

Figure 11- Effect of atomization air flow rate on mean radial velocity profiles in CME fuel spray flames. Uncertainty in these figures is approximately ± 0.2 m/s.
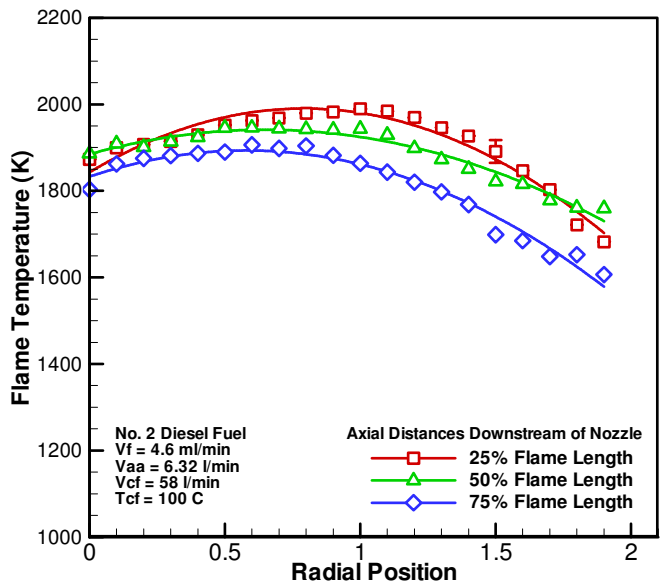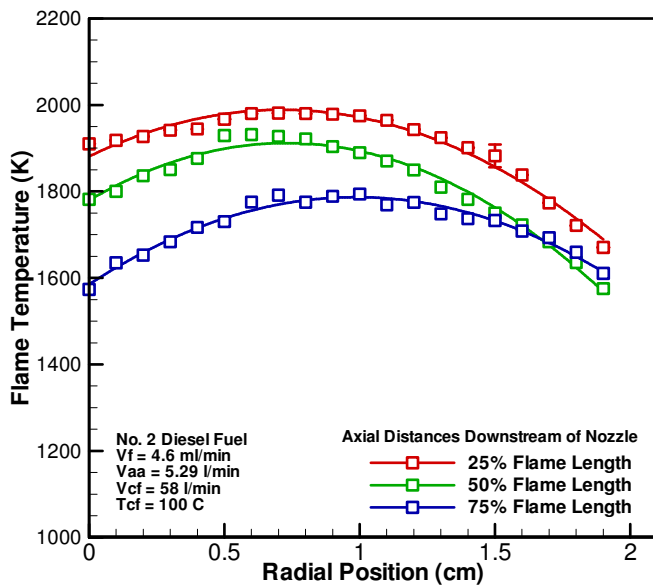

Figure 12- Effect of atomization air flow rate on in-flame temperature profiles of No. 2 D fuel spray flames.

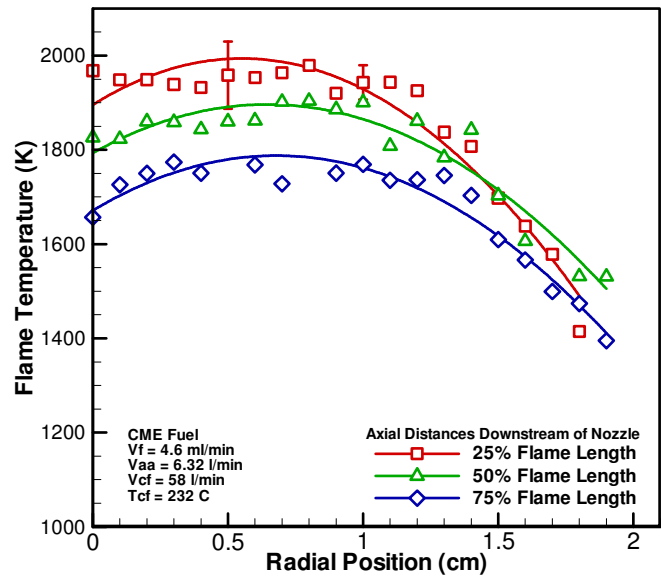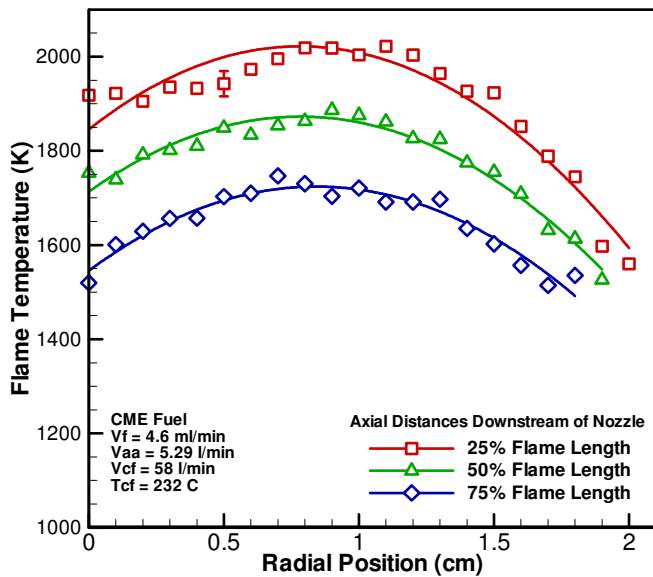10   Copyright © 2008 by ASME

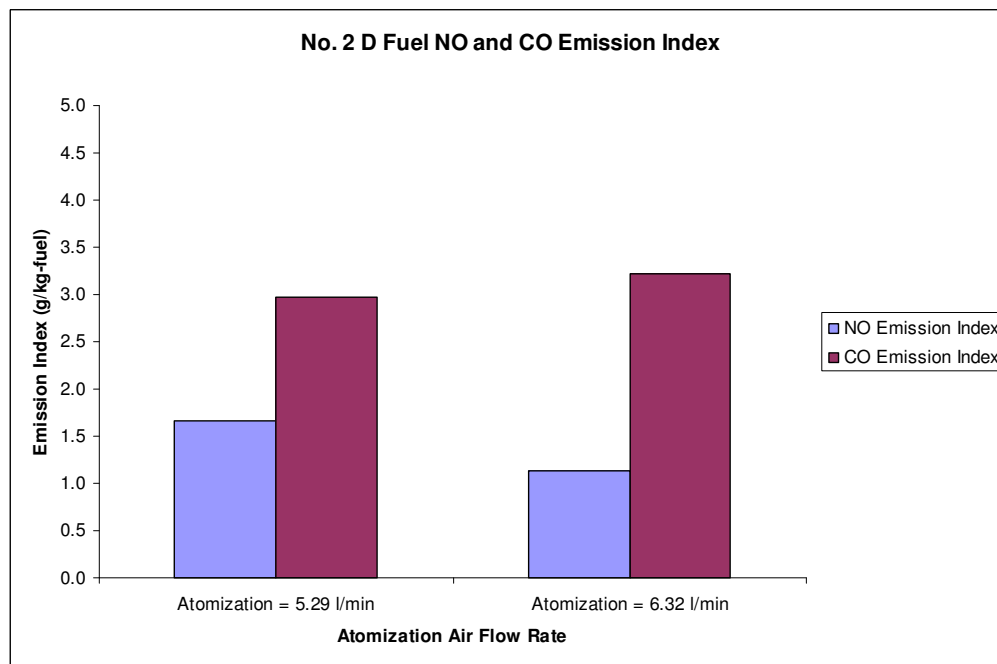Figure 13- Effect of atomization air flow rate on in-flame temperature profiles of CME fuel spray flames.

Figure 14- Effect of atomization air flow rate on global emission index of NO and CO of No. 2 D fuel spray flames.
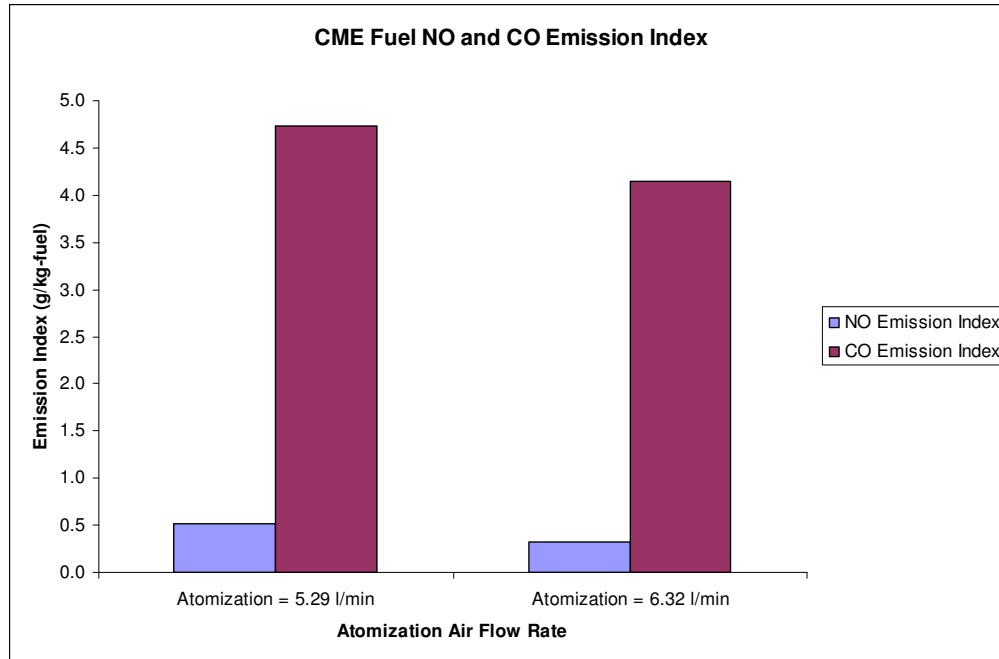
CME Fuel NO and CO Emission Index

Figure 15- Effect of atomization air flow rate on global emission index of NO and CO of CME fuel spray flames.

Table 1- Physical and Chemical Properties of No. 2 Diesel Fuel and Canola Methyl Ester Fuel.

Fuel	Molecular Formula	Density	Boiling Point	Viscosity	Heating Value	Iodine Number
		(kg/m3)	(C)	cost	MJ/kg	
No. Diesel Fuel	$\sim C_{16}H_{34}$	850	150 - 350	4.61 at 25 C	42.6	NA
Canola Methyl Ester	$\sim C_{19}H_{36}O_2$	876	340 - 405	4.37 at 40 C	37.4	97

Table 2- Fuel and Air Flow Rates and Temperature Settings.

	Atomization Air Flow Rate	Co-Flow Air Flow Rate	Co- Flow Air Temperature	Fuel Flow Rate
No. 2 Diesel Fuel	5.29 and 6.32 (l/min)	58 (l/min)	100 C	4.6 (ml/min)
Canola Methyl Ester	5.29 and 6.32 (l/min)	58 (l/min)	232 C	4.6 (ml/min)

12 Copyright © 2008 by ASME